Title

Tsunami Squares simulation of megathrust-generated waves: Application to the 2011 Tohoku Tsunami

Authors

Wilson, John Max
Schultz, Kasey W
Grzan, David
et al.

Publication Date

2020

DOI

10.1016/j.pdisas.2019.100063

Peer reviewed

Tsunami Squares Simulation of Megathrust-Generated Waves: Application to the 2011 Tohoku Tsunami

John Max Wilson, Kasey W. Schultz, David Grzan, John B. Rundle, Steven N. Ward, Ramya Bhaskar, Omer Saeed, Harshita Kaushal

PII: S2590-0617(19)30063-8

DOI: https://doi.org/10.1016/j.pdisas.2019.100063

Reference: PDISAS 100063

To appear in: *Progress in Disaster Science*

Please cite this article as: J. Max Wilson, K.W. Schultz, D. Grzan, et al., Tsunami Squares Simulation of Megathrust-Generated Waves: Application to the 2011 Tohoku Tsunami, *Progress in Disaster Science*(2019), https://doi.org/10.1016/j.pdisas.2019.100063

Tsunami Squares Simulation of Megathrust-Generated Waves: Application to the 2011 Tohoku Tsunami

John Max Wilson[a,*], Kasey W. Schultz[a], David Grzan[a], John B. Rundle[a,b], Steven N. Ward[c], Ramya Bhaskar[a], Omer Saeed[a], Harshita Kaushal[a]

[a]*Department of Physics, University of California, Davis, CA 95616*
[b]*Department of Earth and Planetary Sciences, University of California, Davis, CA 95616*
[c]*Department of Earth and Planetary Sciences, University of California, Santa Cruz, CA 95064*

Abstract

Large subduction zone earthquakes often cause tsunamis, but observational data for hazard analysis is limited. Synthetic catalogs of seismically-generated tsunami scenarios can be created by pairing earthquake and wave simulations. Tsunami Squares is one such wave simulator, explicitly tracking water mass and momentum, allowing simulation of dry land and the inundation process. We demonstrate a C++ port of Tsunami Squares paired with the Virtual Quake simulator by replicating the 2011 Great East Japan Earthquake and Tsunami. Comparisons of coastal run-up and wave heights with observations finds good agreement, with future improvements coming from tsunami source time dependence.

Keywords: Tsunami Squares, simulation, hazard analysis

1. Introduction

Tsunamis present unique threats as natural disasters, because they are often accompanied by damage from the earthquakes or landslides that caused them. Seismic tsunamis are most often associated with large earthquakes in subduction zones. During such events, shifts in overhanging crustal slabs cause large seafloor displacements, resulting in corresponding displacements of water. As the ocean surface returns to equilibrium, these displacements propagate outward as tsunamis.

*Corresponding author, email: jhnwilson@ucdavis.edu
[1]Declarations of interest: none

There are many examples of massive loss of life and property as a result of seismic tsunamis in the Indo-Pacific region, with many of the highest-risk areas located in the developing world. Indonesia (Ammon et al., 2005; Lay et al., 2005), Cascadia (Satake et al., 1996; Nelson et al., 2006), Alaska (Shennan et al., 2009), and Chile (Fujii and Satake, 2013) all feature subduction regions capable of producing tsunamis at a scale devastating to humans.

Numerical wave simulations are powerful tools for understanding tsunami hazard in at-risk areas. To reduce the impact of future disasters, physics-based simulations will play a vital role in statistical hazard analysis and tsunami early warning systems. Pre-computed catalogs of synthetic tsunamigenic earthquakes and their resulting tsunamis, their inundation risks, and their observable warning signs can be used to identify hazards in time to issue warnings to threatened communities. Towards this goal, we introduce a simulator pipeline for tsunamigenic earthquakes and the coastal inundations they produce. We pair the Virtual Quake (Sachs et al., 2012; Schultz et al., 2018) long-term earthquake simulator with the Tsunami Squares wave simulator (Xiao et al., 2015; Wang et al., 2015b,a).

Typical far-field tsunami simulations employ the shallow water approximation of the Navier-Stokes fluid flow equations, the most common approach being some form of finite-difference method (Imamura, 1996). Tsunami Squares is an alternative numerical simulation algorithm. Originally developed in Fortran as a method for simulating landslide-induced tsunamis, Tsunami Squares is capable of seamlessly simulating dry land and inundation. With the goal of greater interoperability with other software, we introduce a C++ port of Tsunami Squares.

For proof of concept and validation purposes we recreate the 2011 Tohoku Earthquake and Tsunami. While Virtual Quake is not used to generate synthetic earthquakes in this study, the inferred subduction slab slip from the 2011 event is fed into Virtual Quake to recreate seafloor displacements, which are then used as initial conditions for a Tsunami Squares wave simulation. We compare waveforms and inundation to observations. We also compare the Virtual Quake/Tsunami Squares results to waveforms produced using an established simulator, the Regional Ocean Modeling System (`https://www.myroms.org`).

2. Great East Japan Earthquake and Tsunami

On March 11, 2011, at 2:46 pm local time, a large slip event occurred in the Japan Trench roughly 72 km east of the Tohoku coast, where the Pacific plate subducts under the North American plate. The event lasted for six minutes, with maximum slips of up to 60 m over an area of $60,000\text{km}^2$, and would eventually be categorized as a magnitude 9.1 earthquake. (Hayes et al., 2017). The quake had been preceded by several $M > 6.0$ foreshocks in the prior three days.

This earthquake, which represented the largest in recorded Japanese history, had a relatively shallow hypocentral depth of 25 km, and resulted in tsunamigenic sea floor displacement. The initial inundations resulting from the tsunami occurred roughly 10 minutes after the earthquake, with the most damaging inundation of the Sendai Plain continuing to occur an hour after the earthquake. The wave heights reached up to 35 meters, overwhelming the country's safeguards. The disaster resulted in an estimated death toll of 16,000 and caused approximately $210 billion in damages (Able M, 2012; Mori et al., 2012).

The Great East Japan Earthquake and Tsunami in many ways represents a worst-case natural hazard occurring in a country with best-case disaster risk reduction practices. The nonetheless great losses of life and property were in part accountable to a lack of preparedness for the least-likely scenario. Along with the wealth of observational data from – and analyses of – the event, this becomes an attractive case study for developing a pipeline for statistical hazard analysis and early warning.

3. Tsunami Squares

3.1. Shallow Water Model

Typical tsunami flow calculations are performed by solving nonlinear long wave continuity equations. For a two-dimensional model with wave propagation through locations $\boldsymbol{r} = (x, y)$, in which water height is represented by the scalar $H(\boldsymbol{r}, t)$ and height-averaged velocity as $\boldsymbol{v}(\boldsymbol{r}, t)$:

$$\frac{\partial H(\boldsymbol{r}, t)}{\partial t} = -\nabla \cdot \big(\boldsymbol{v}(\boldsymbol{r}, t) H(\boldsymbol{r}, t)\big) \tag{1}$$

and

$$\frac{\partial H(\boldsymbol{r},t)\boldsymbol{v}(\boldsymbol{r},t)}{\partial t} = -\nabla \cdot \big(\boldsymbol{v}(\boldsymbol{r},t)\boldsymbol{v}(\boldsymbol{r},t)H(\boldsymbol{r},t)\big) - gH(\boldsymbol{r},t)\nabla\zeta(\boldsymbol{r},t) \tag{2}$$

Here g is the gravitational acceleration, $\zeta(\boldsymbol{r},t)$ is the elevation of the water, and t is time. For a small, discreet time step dt, Equations 1 and 2 can be rewritten as

$$H(\boldsymbol{r},t+dt) = H(\boldsymbol{r},t) - \nabla \cdot (\boldsymbol{v}(\boldsymbol{r},t)H(\boldsymbol{r},t))\,dt \tag{3}$$

$$\begin{aligned} H(\boldsymbol{r},t+dt)\boldsymbol{v}(\boldsymbol{r},t+dt) =& H(\boldsymbol{r},t)\boldsymbol{v}(\boldsymbol{r},t) - \nabla \cdot \big(\boldsymbol{v}(\boldsymbol{r},t)\boldsymbol{v}(\boldsymbol{r},t)H(\boldsymbol{r},t)\big)dt \\ & - gH(\boldsymbol{r},t)\nabla\zeta(\boldsymbol{r},t)dt \end{aligned} \tag{4}$$

3.2. Tsunami Squares Wave Model

The Tsunami Squares method solves equivalent equations by explicitly propagating mass and momentum across a grid of N cells with, for some cell i, center points $\boldsymbol{r}_i$, area A_i, and topographic altitude T_i. At time t, each cell contains a column of water of height $H_i(t)$, with vertically-averaged horizontal velocity $\boldsymbol{v}_i(t))$ and mean horizontal acceleration of $\boldsymbol{a}_i(t)$. The mass associated with each cell is $m_i(t) = \rho_w A_i H_i(t)$ (where ρ_w is the density of water), and the momentum associated with each cell is $\boldsymbol{p}_i(t) = m_i(t)\boldsymbol{v}_i(t)$. Dry land is simply represented as cell with $H_i(t) = 0$.

To begin a time step, the acceleration is calculated for each cell. We consider acceleration due to gravity and internal fluid drag. Gravitational acceleration is proportional to the gradient of the altitude of the top surface of the water, $\zeta_i(t)$:

$$\boldsymbol{a}_{i\,\mathrm{grav}}(t) = -\nu g \nabla \zeta_i(t) = -\nu g \nabla (T_i + H_i(t)) \tag{5}$$

where ν is a tuning parameter. Working against the direction of motion is frictional acceleration resulting from bulk material motion. This scales with the square of velocity:

$$\boldsymbol{a}_{i\,\mathrm{frict}}(t) = -\mu_d \frac{|\boldsymbol{v}_i(t)|}{H_i(t)} \boldsymbol{v}_i(t) \tag{6}$$

where μ_d is a dynamic frictional coefficient for the material representing velocity-dependent particle interaction. Frictional acceleration acts in opposition to velocity,

but is never allowed to reverse the direction of flow. The total acceleration acting on a simulation cell is

$$\boldsymbol{a}_i(t) = \boldsymbol{a}_{i\,\mathrm{grav}}(t) + \boldsymbol{a}_{i\,\mathrm{frict}}(t) \tag{7}$$

Wave propagation simulation proceeds as illustrated in Figure 1. The water in each square is moved according to its velocity and acceleration, such that the water's new center point is located at

$$\tilde{\boldsymbol{r}}_i = \boldsymbol{r}_i + \boldsymbol{v}_i(t)dt + \frac{1}{2}\boldsymbol{a}_i(t)dt^2 \tag{8}$$

while its velocity and momentum are updated to

$$\tilde{\boldsymbol{v}}_i = \boldsymbol{v}_i(t) + \boldsymbol{a}_i(t)dt \tag{9}$$

After it moves, water from source-cell i will overlap with other simulation cells, which will receive whatever water overlaps their area. For receiving-cell j, the overlap proportion is denoted as $\delta A_{ij}(t)$. Mass and momentum is distributed to those cells according to the proportion of overlap.

$$H_j(t+dt) = \sum_i H_i(t)\delta A_{ij} \tag{10}$$

The momentum is similarly distributed:

$$\boldsymbol{p}_j(t+dt) = \sum_i \tilde{\boldsymbol{p}}_i \delta A_{ij} = \sum_i \rho_w A_i H_i(t) \tilde{v}_i \delta A_{ij} \tag{11}$$

and the new velocity associated with each cell is calculated

$$\boldsymbol{v}_j(t+dt) = \frac{\boldsymbol{p}_j(t+dt)}{\rho_w A_i H_i(t+dt)} \tag{12}$$

Because this method tracks volume and momentum from each time step to the next, these quantities are naturally conserved during simulation, enforcing

$$\sum_i^N H_i(t+dt) = \sum_i^N H_i(t) \tag{13}$$

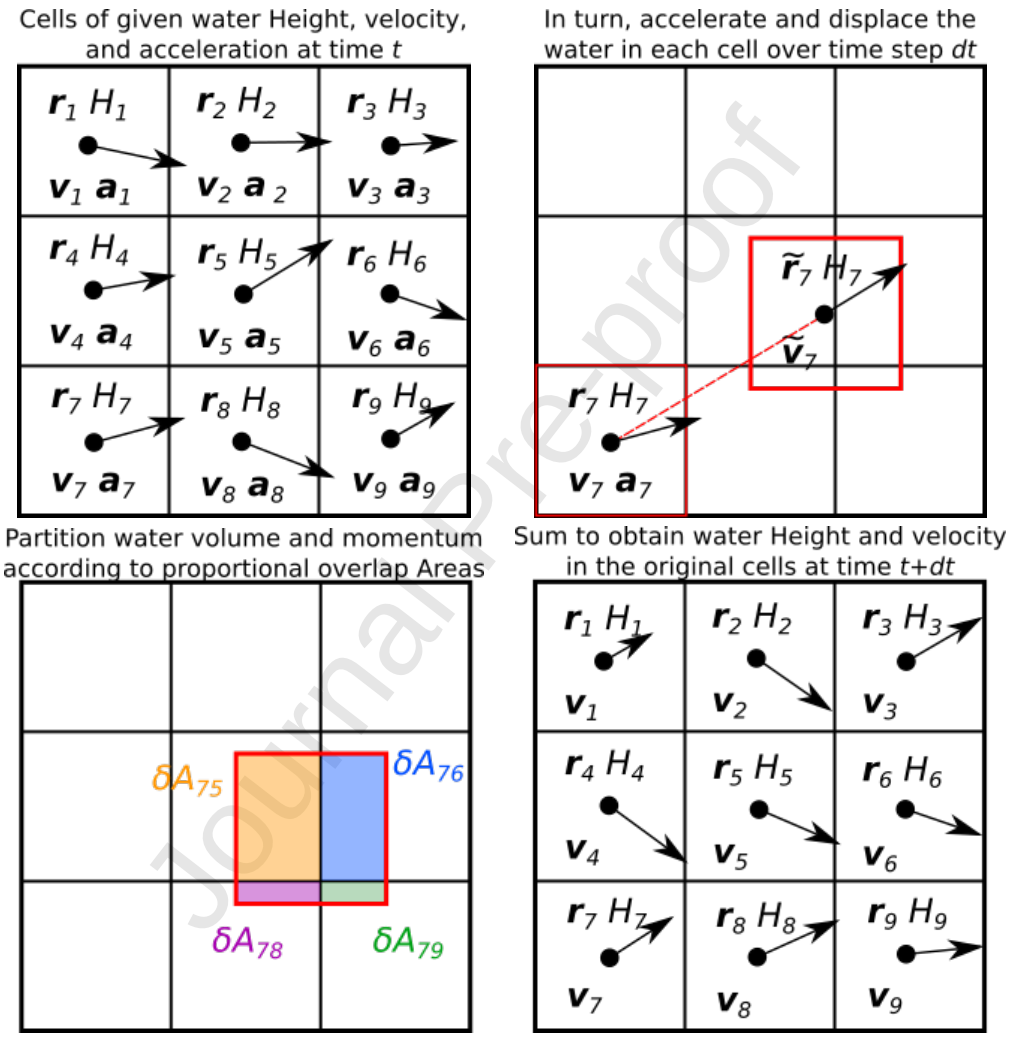

Figure 1: Tsunami Squares wave propagation concept

$$\sum_{i}^{N} \boldsymbol{p}_i(t+dt) = \sum_{i}^{N} \boldsymbol{p}_i(t) \tag{14}$$

Other fluids may be added to the simulation, for example mud in the case of a landslide. This requires frictional interactions with topography and other simulated materials, along with unique densities and internal frictional losses. Each time step, each material goes through an identical redistribution process to that outlined above, with momentum transferring between layers of materials. The C++ implementation of Tsunami Squares currently only supports simulation of water over topography.

3.3. Simulation

The basic program flow of Tsunami Squares is illustrated in Figure 2. Tsunami Squares begins by reading a file containing the combined topography/bathymetry of the region to be simulated. This defines the location, size, and altitude of each interacting square. Currently, the ETOPO1 combined bathymetry/topography map provided by the National Oceanic and Atmospheric Association ([dataset] Amante and Eakins, 2009) is used to define the pre-event sea floor at 1 arc minute resolution. Each square is filled with water up to sea level, with no water being added initially to squares above sea level. The initial conditions of the simulation are then set according to one of three options:

1. Vertically displacing the topography of each square according to a provided displacement file. Such displacements might be modeled from an earthquake. These seafloor displacements propagate to the surface of the water, providing a nonzero water surface gradient for square accelerations.
2. Reading a previously-generated tsunami simulation output file, allowing simulations to be resumed. Simulation can be resumed on the same or different topographic grid.
3. Placing a Gaussian-distributed pile of water on top of the ocean surface. This is used for physics verification purposes, as described in further detail in Section 3.5.

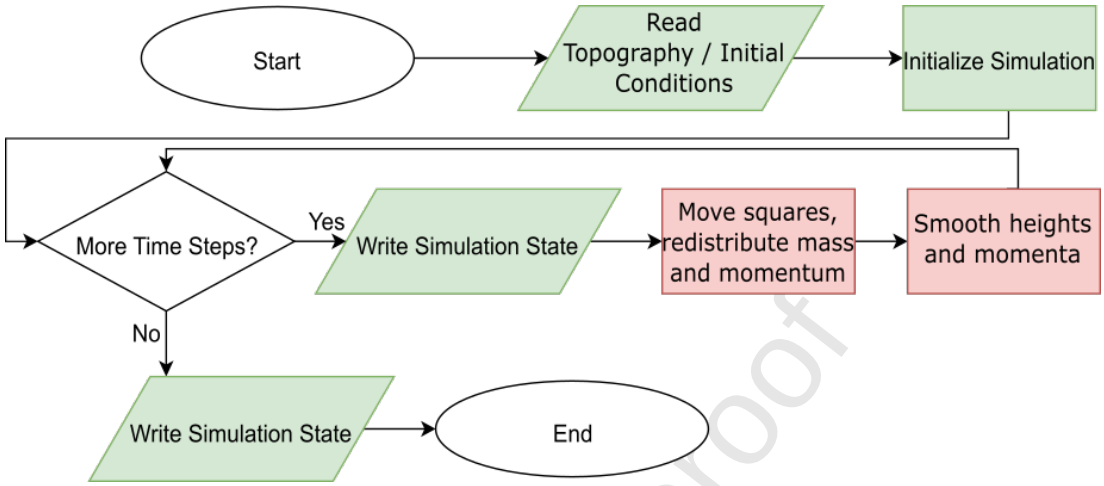

Figure 2: Tsunami Squares simulation flow chart. Red blocks indicate parallelized code.

After the simulation is initialized, the loop over time steps is entered. In each loop, the simulation state is written to the output file, squares are accelerated and moved, according to the physics of Section 3.2, and the heights and momenta of the squares is smoothed. When all time steps have been simulated, the final simulation state is written and the program terminates.

In methods like Tsunami Squares, smoothing is an important step to avoid non-physical artifacts of the discrete simulation. In Tsunami Squares, this is accomplished by comparing the water heights and momenta in each square to those of its nearest neighbors. For each neighbor, the square with more water lends $\delta_{smooth} * \left|(H_{self} - H_{neighbor})\right|$ to the neighbor with lower height, where

$$\delta_{smooth} = 0.15 * \min\left(0.02 + 0.125 * \left(\frac{H(\boldsymbol{r},t)}{6000}\right), 0.5\right) \tag{15}$$

Likewise, the square with more momentum contributes $\delta_{smooth} * \left|(\boldsymbol{p}_{self} - \boldsymbol{p}_{neighbor})\right|$ to the lower-momentum square. The form of Equation 15, as well as its constants, was chosen for best performance across many different heights of water. The height dependence causes smoothing to be stronger in deeper water, and less effective near coasts, where variations in height and momentum between neightboring water columns

are important for accurate inundation simulation. The min operation ensures that no more than 7.5% of the height or momentum difference is traded between squares each smoothing pass. The volume and momentum exchanges are calculated in parallel and then distributed to prevent a directional bias in smoothing. This, however, results in the occasional over-drawn square, which must be avoided to prevent simulation crashes (there's no such thing as negative amounts of water). Therefore, these "overdrafts" are filled back in, and the overall volume of water in the simulation is normalized such that total volume is conserved. Several smoothing passes each time step are usually necessary to produce artifact-free simulations, though the minimum necessary number of passes should be used.

3.4. C++ Port

The original implementation of the Tsunami Squares algorithm was written in Fortran by Ward (Xiao et al., 2015; Wang et al., 2015b,a). The algorithm has been rewritten in the widely-used language C++ for ease of use for a broader audience and interoperability with other software. Additional functionality has also been added:

1. The ability to load a previous simulation on a different-sized simulation grid, allowing waves distant from shore to be simulated on a coarser, computationally efficient grid, and then transitioned to a finer-resolution grid for accurate inundation simulation.
2. Use of the GeographicLib and Boost Geometry libraries, providing accurate distance and overlap calculations on a spherical or ellipsoidal Earth.
3. Parallelization of the most computationally intense sections of the code using OpenMP, allowing performance gains for users with multiple computational threads available.

3.5. Verification

In order to verify that the simulated waves are physically accurate, the output of the initial conditions of a Gaussian-distributed pile of water over a flat ocean bottom is compared to a semianalytic solution (Ward, 2011).

For such Gaussian-pile initial conditions, the initial displacement from sea level of the ocean surface is written as $u_z^{\text{surf}}(\boldsymbol{r},0) = D_c \exp^{(}-r^2/R_c^2)$, and the displacement at time t is

$$u_z^{\text{surf}}(\boldsymbol{r},t) = \int_0^\infty \frac{kdk}{2\pi} \cos[\omega(k)t] \mathrm{J}_0(kr) \mathrm{F}_0(k) \tag{16}$$

where J_0 is the zeroth Bessel function of the first kind, $\omega(k) = \sqrt{gk\tanh(kH)}$ is the dispersion relation for ocean depth H, and

$$F_0(k) = \pi D_c R_c^2 \exp\left[-(kR_c/2)^2\right] \tag{17}$$

Figure 3 shows the performance of Tsunami Squares starting with the Gaussian-pile initial conditions, demonstrating good agreement between the two.

Figure 4 shows an analytic sinusoidal solution to Equations 1 and 2, for a wave interacting with a sharp bathymetric step from a depth of 1000m to 500m. A Tsunami Squares simulation of a sinusoidal wave packet was performed on an identical bathymetry, and the results show identical reflection and transmission at the boundary.

Tsunami Squares also shows good agreement with traditional finite difference simulations of the shallow water equations. Figure 5 features the finite difference simulation of Equations 3 and 4 for an initial rectangular uplift of water, as well as a Tsunami Squares simulation with identical initial conditions and smoothing algorithm.

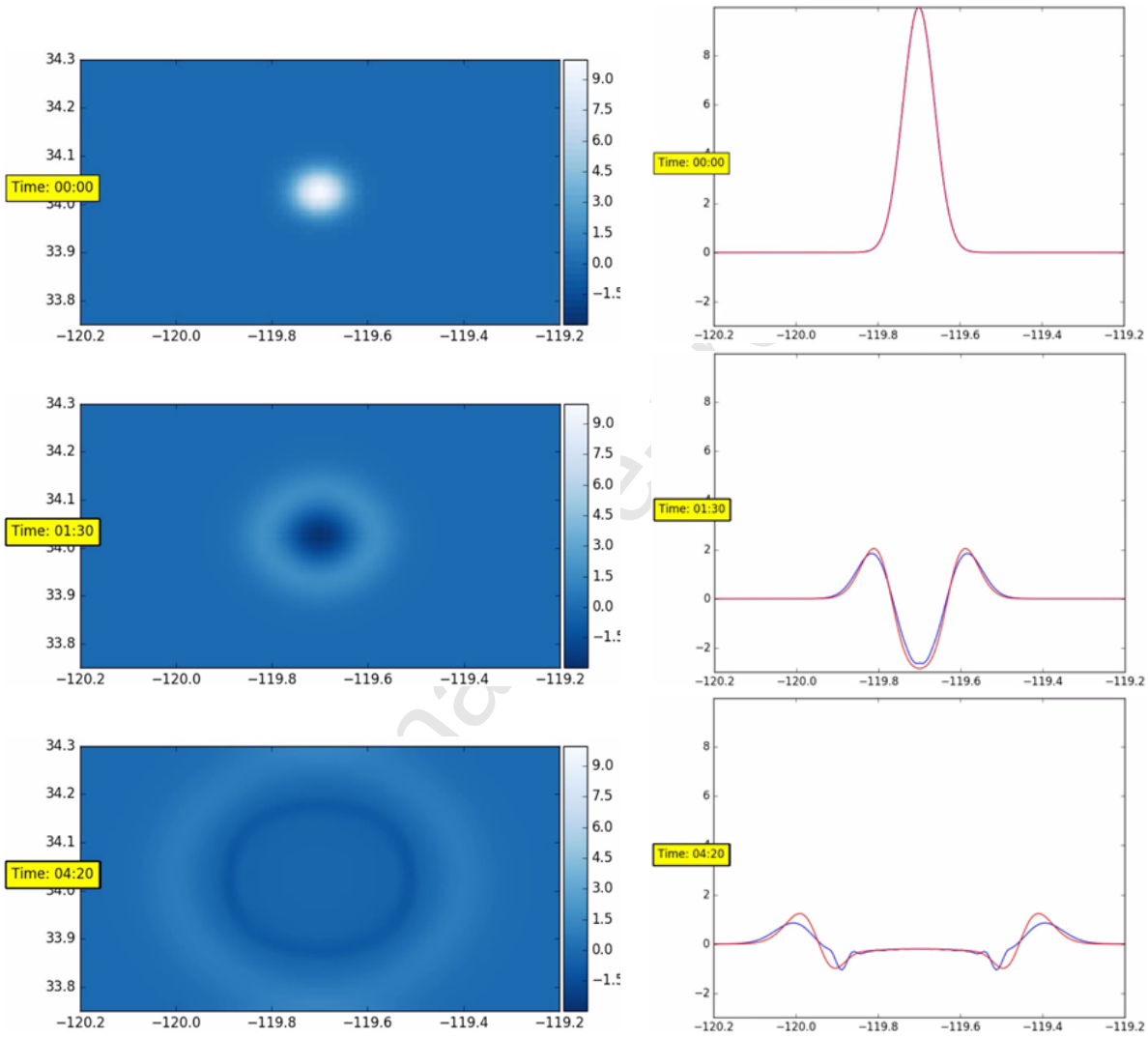

Figure 3: Gaussian-pile initial conditions for verification over a flat bathymetry with depth of 1 kilometer, with pile central height of 10 meters, and standard deviation of 5 kilometers. **Left Column:** Overhead view of simulation, with color scale representing water height in meters. **Right Column:** Height vs. longitude for cross section centered on the simulation. Red curve is semi-analytic solution, blue curve is simulation output. Latitude and longitude in all plots are used for distance calculations but are otherwise arbitrary. Time is in Minute:Second format.

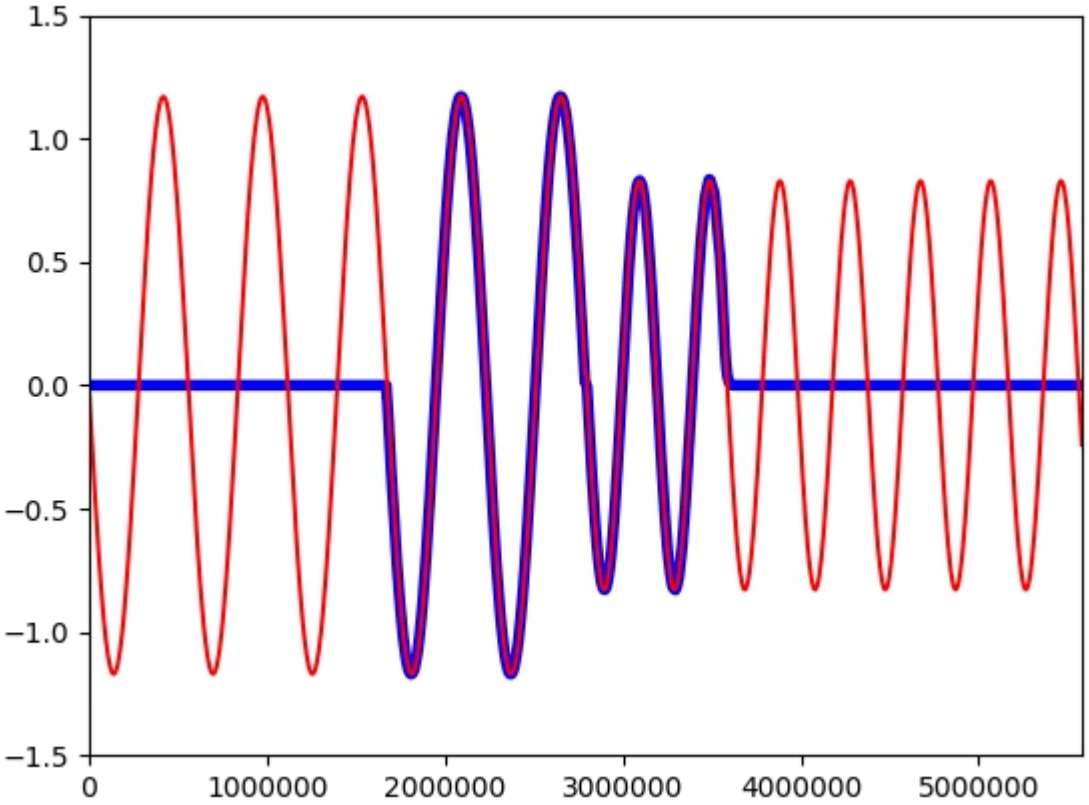

Figure 4: Comparison between the analytical solution to the shallow water equations of a sinusoidal wave passing over a jump in bathymetric depth from 1000m to 500m (red), and a Tsunami Squares simulation of a sinusoidal wave packet traveling over the same jump in depth (blue). Axes units are in meters.

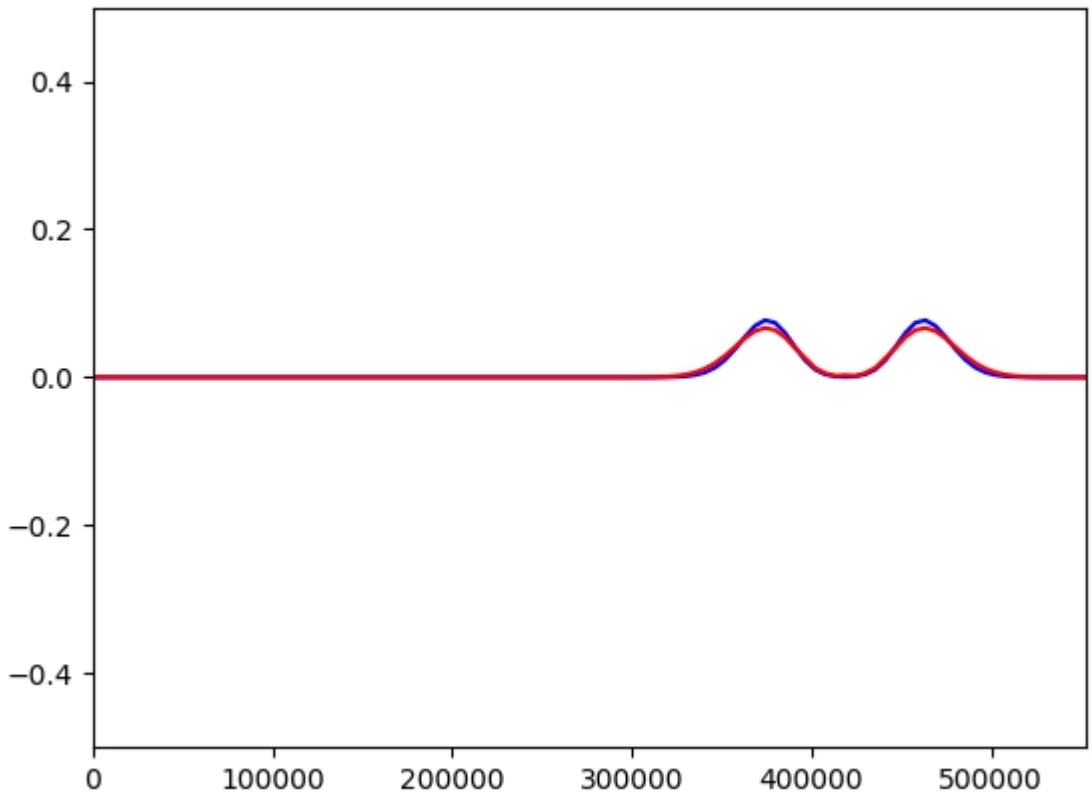

Figure 5: Comparison between finite difference simulation of the shallow water equations (blue line) and a Tsunami Squares simulation (red). Both simulations feature the same smoothing algorithm and initial rectangular uplift. Axes units are in meters.

4. Sea Floor Uplift Calculation

For calculating the initial uplift of the sea floor due to the 2011 Tohoku Earthquake, we use the Virtual Quake software package. Virtual Quake is an open source software hosted by the Computational Infrastructure for Geodynamics (CIG, `https://geodynamics.org/cig/software/vq/`), and version controlled through github (`https://github.com/geodynamics/vq`).

Virtual Quake models the earth's crust as a homogeneous linearly elastic halfspace. Faults are modeled as planar surfaces, representing discontinuities in that halfspace. These are divided into smaller squares, or elements. These fault elements represent the fundamental interacting pieces of the simulation, analogous to each sliding block of the slider block model of Rundle and Jackson (1977).

Each fault element interacts with all others through elastic stress transfer, governed by quasi-static Green's functions (Okada, 1992). For each unit of slip, elements transfer shear and normal stresses to each other depending on their relative positions and orientations.

For indices running over the three Cartesian coordinates, the stress tensor change σ_{ij} at a location $\boldsymbol{x}$ due to influences from all other locations $\boldsymbol{x'}$ is given by Rundle et al. (2006)

$$\sigma_{ij}(\boldsymbol{x},t) = \int dx'_k T^{kl}_{ij}(\boldsymbol{x}-\boldsymbol{x'}) s_l(\boldsymbol{x'},t) \tag{18}$$

where $s_l(\boldsymbol{x'},t)$ is the amount of slip in direction l, and $T^{kl}_{ij}(\boldsymbol{x}-\boldsymbol{x'}$ is the Green's function tensor.

Virtual Quake allows access to much of its functionality, including Okada Green's function stress and displacement equations, through the QuakeLib library. To reproduce the surface displacement caused by the Tohoku earthquake, we apply these tools to the slip distribution and fault model of Satake et al. (2013), as shown in Figure 6. The result is the vector displacement of the Earth's surface following the earthquake (Figure 7). The vertical component of this displacement constitutes the initial conditions for the ensuing tsunami simulation.

Currently, the initial seafloor uplift occurs instantaneously at the beginning of a Tsunami Squares simulation. Large subduction earthquakes actually rupture over the

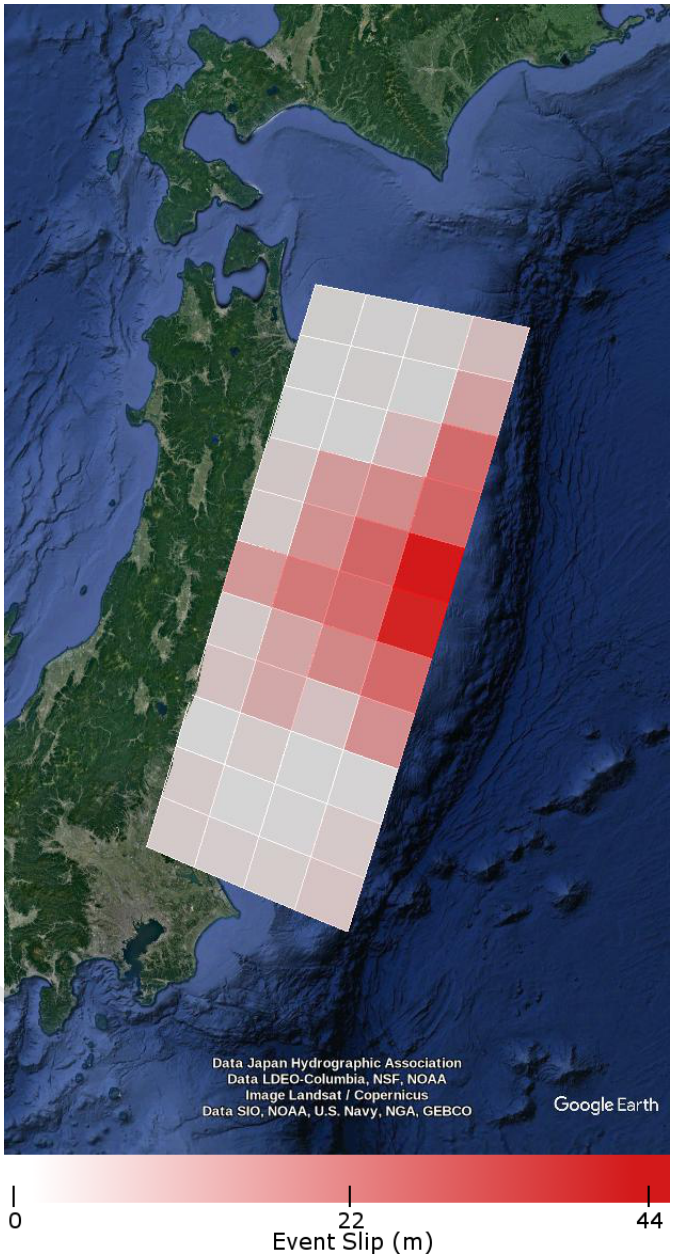

Figure 6: Fault geometry of the subduction zone involved during the 2011 Tohoku earthquake and tsunami, as seen from a birds-eye view in Google Earth. Color indicates slip amount during that event, with maximum slip near the trench of 44 meters, as calculated by Satake et al. (2013).

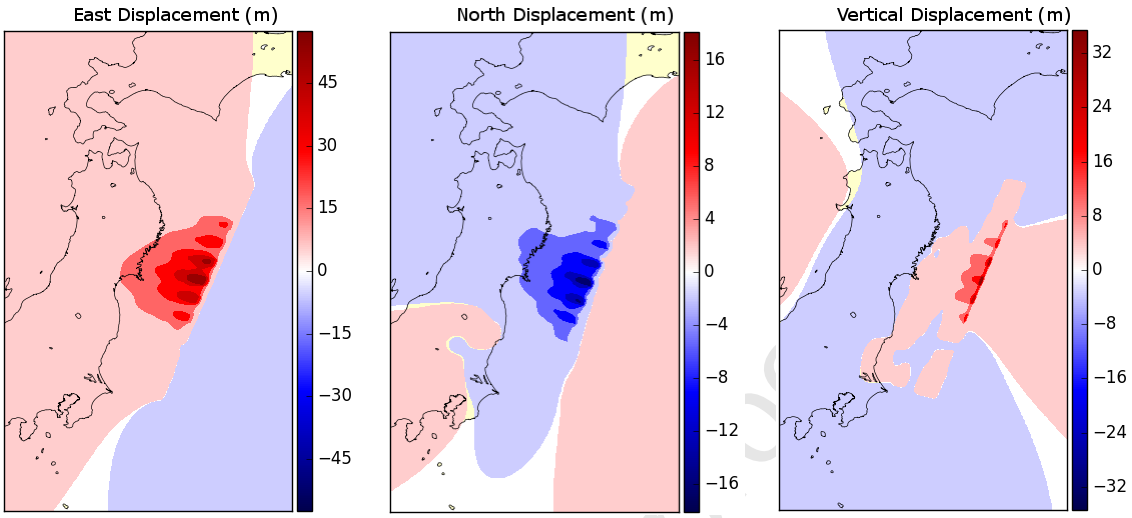

Figure 7: Easterly, northerly, and vertical surface displacements resulting from the slip distribution of Satake et al. (2013), as calculated by the Okada (1992) elastic half-space deformation Green's functions packaged with Virtual Quake. Note the different color scales for each displacement map.

course of several minutes; incorporation of time-dependence to the uplift source model are planned for future Tsunami Squares development.

5. Simulation Results

The simulation was initialized in the large region shown in Figure 7. The native one arc minute spatial resolution of the ETOPO1 bathymetry dataset was used, with a two second temporal resolution. The gravitational acceleration tuning parameter was set to $\nu = 0.5$. At this resolution, four smoothing passes were used each time step. The wave was allowed to propagate for 800 simulated seconds.

After 800 seconds, the wave front was close to making landfall, so the simulation was transitioned to the smaller region shown in Figure 8 at twice the linear resolution (interpolated from the one arc minute resolution ETOPO1 bathymetry dataset.), chosen to include the Sendai basin and region of first landfall. The simulation then continued for an additional 6000 seconds until maximum inundations had been observed for the simulation region, for a total simulation time of 113 minutes. At this resolution, six smoothing passes were performed each time step.

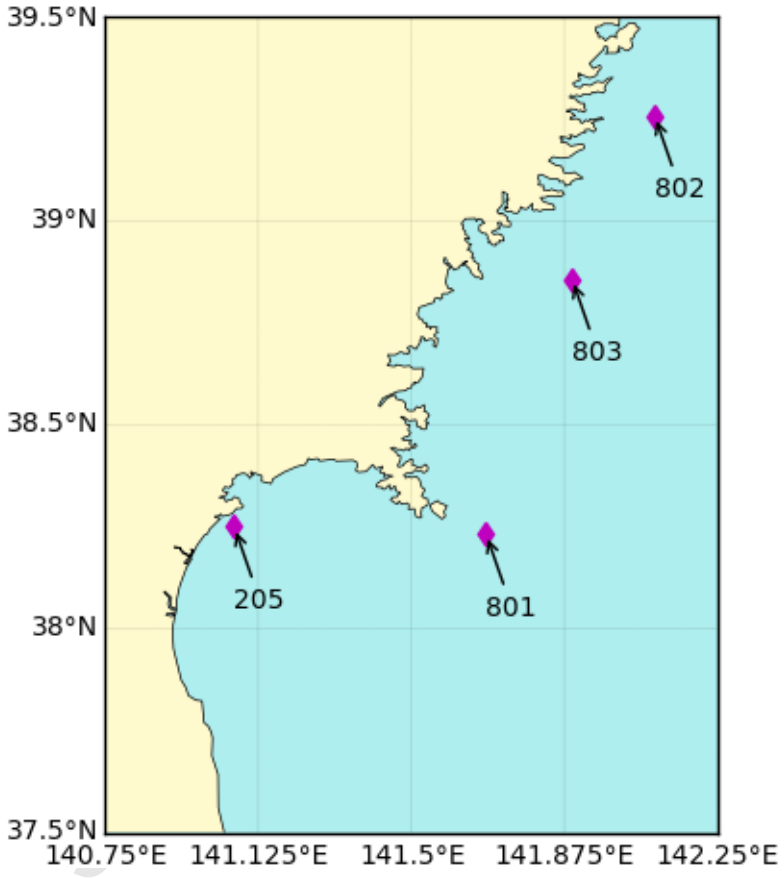

Figure 8: Locations of the NOWPHAS wave monitoring buoys, labeled with their Point Codes, contained within the simulated region off the coast of the Tohoku region in Japan for which five second resolution data during the 2011 Tohoku earthquake and tsunami exists.

Point Code	Description	Latitude	Longitude	Type
205	Sendai-Shin-Kou (Sendai New Port)	38°15′00″	141°03′58″	Coastal wave gauge
801	Miyagi-Chubu-Oki (Central Miyagi)	38°13′57″	141°41′01″	GNSS buoy
802	Iwate-Nanbu-Oki (South Iwate)	39°15′31″	142°05′49″	GNSS buoy
803	Miyagi-Hokubu-Oki (North Miyagi)	38°51′28″	141°53′40″	GNSS buoy

Table 1: NOWPHAS instruments used in wave height comparison between Tsunami Squares recreation of 2011 Tohoku tsunami and five second resolution observational data.

The Port Authority of the Ministry of Land, Infrastructure and Transport of Japan administers a system of instruments along the Japanese coast for measuring wave properties, the Nationwide Ocean Wave information network for Ports and HArbourS (NOWPHAS) ([dataset] Real-time NOWPHAS, 2011). The buoys contained within the simulated off-coast region used for this comparison are listed in Table 1.

5.1. Waveform Analysis and Comparison to ROMS

Figure 9 shows a comparison between the wave forms of the NOWPHAS buoy observations, Tsunami Squares simulation, and a simulation performed by Song et al. (2017) using the Regional Ocean Modeling System (ROMS) (`https://www.myroms.org`). Because the smoothing algorithms used in simulation constitute a low-pass filter on the simulated waveform, we apply a fifth-order Butterworth low-pass filter on the observed height data.

ROMS is an open-source tsunami model, which has been modified here with simplified ocean physics. Water is assumed to have constant density (as in Tsunami Squares). The horizontal resolution is about 5 km, with 30 levels of vertical resolution. Song et al. (2017) incorporate kinetic and potential energy imparted by the horizontal seafloor displacement, and used in-situ GNSS measurements of seafloor displacement as the initial condition of the ROMS simulation.

As a measure of agreement between simulation and observation, we follow Aida (1978). The amplitudes of the buoy observation x_i for the first and second half-cycles (Leading tsunami wavefront peak and trough), as well as the wave arrival times, t_{0i}, are

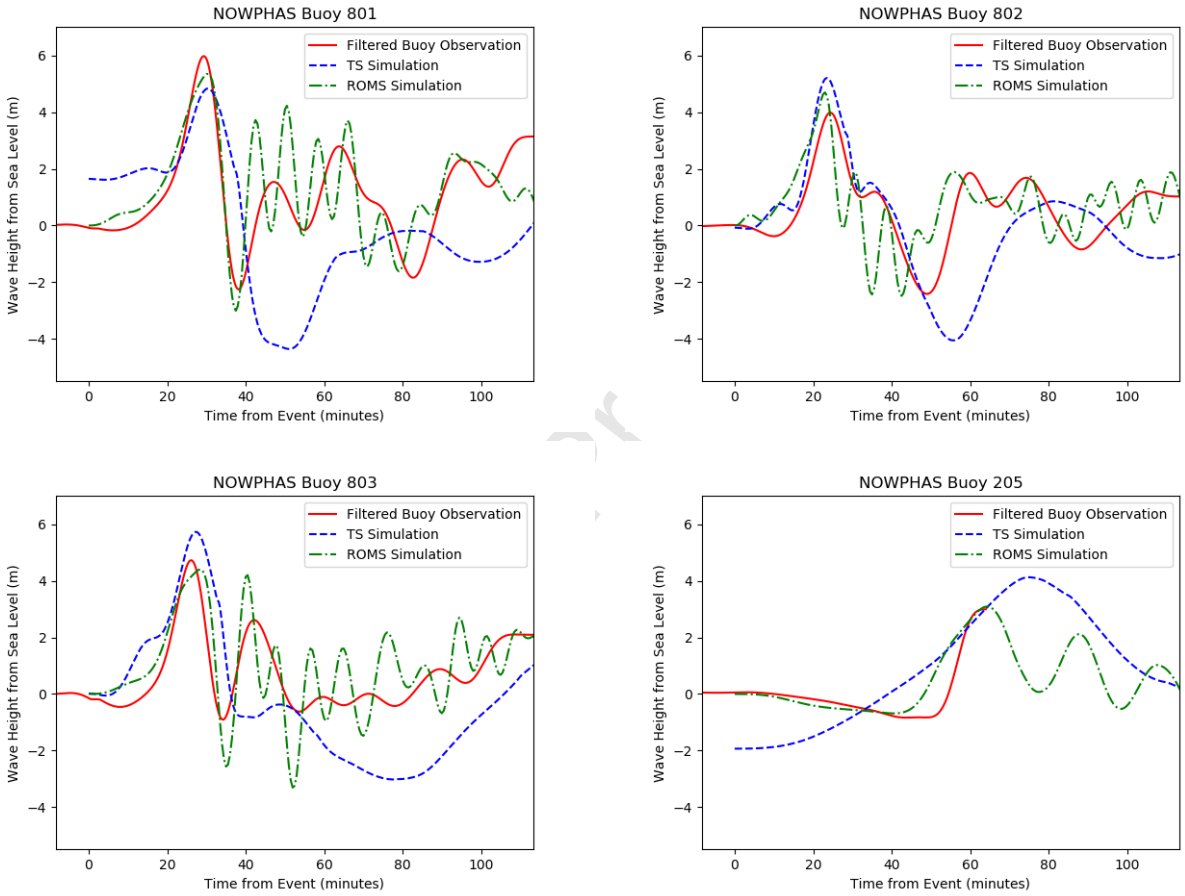

Figure 9: Comparison between filtered observed wave heights during the 2011 Tohoku tsunami (red solid line), a Tsunami Squares simulation (blue dashed line), and the ROMS simulation (green dash-dot line) at the location of the NOWPHAS wave monitoring buoys. A low-pass filter has been applied to the observed waveform, matching the low-pass effect of the smoothing algorithm present in the simulation.

Model	a_1		a_2		t_{0-c}	τ
	K	κ	K	κ		
Tsunami Squares	0.87	1.23	0.70	1.39	-3.08	4.63
ROMS	1.00	1.11	0.64	1.54	-0.67	1.35

Table 2: K, κ, t_{0-c}, and τ calculated for Tsunami Squares and ROMS

found for each buoy i. Similar quantities are found for simulation: y_i and t_c. We define $K_i = x_i/y_i$, representing a correction factor for the simulated amplitude. The geometric average over observation points, K, is found:

$$\log(K) = \frac{1}{n}\sum_{i}^{n} \log K_i \tag{19}$$

A factor κ, representing fluctuation in K_i over the different buoys, is found:

$$\log \kappa = \left[\frac{1}{n}\sum_{i}^{n} \log(K_i)^2 - \log(K)^2\right]^{\frac{1}{2}} \tag{20}$$

The mean difference in observed and simulated arrival times across all four buoys, t_{0-c}, as well as its standard deviation, τ, is found. Table 2 shows the calculated values for both Tsunami Squares and ROMS. These are plotted in Figure 10, with κ and τ represented as error bars. Because data for buoy 205 is unavailable after the first wave peak, buoy 205 does not contribute to K or κ for the second half-cycle.

Similar performance in the amplitude correction factor K is seen for Tsunami Squares as for ROMS, with both simulators performing well. The notable difference in performance is in the arrival times, t_{0-c}. Figure 9 shows that, while Tsunami Squares has accurate arrival times for three of the buoys closest to the initial uplift, the wave-front is too late reaching the farthest buoy, 205. This indicates the gravitational acceleration parameter, ν, is tuned low. Stronger gravitational accelerations were experimented with (not shown here), resulting in far lower arrival time error τ, but which arrived at each station many minutes too early. This indicates that the most valuable future improvement to the C++ port of Tsunami Squares is the implementation of time-dependence in the tsunami source, allowing for accurate arrival times at full-strength gravitational accelerations.

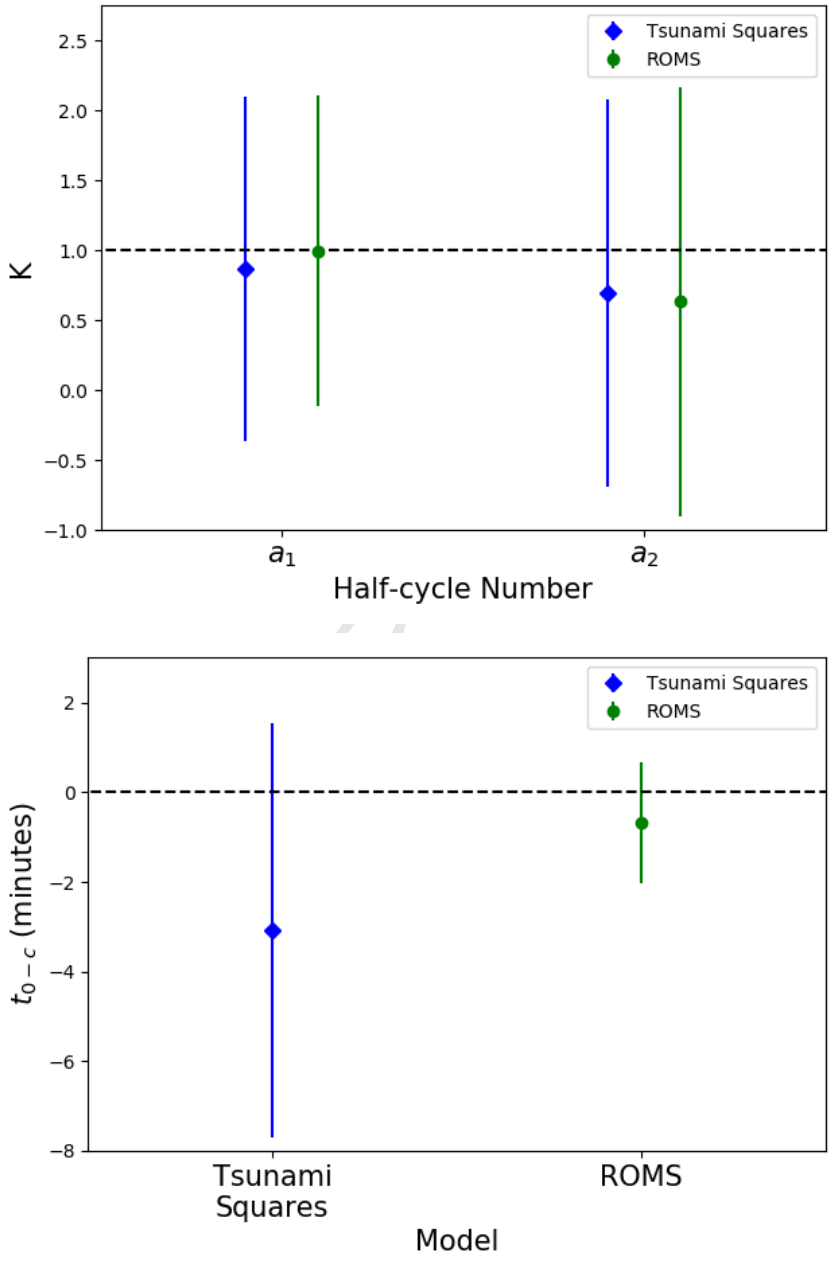

Figure 10: K for the first two half-cycles of the tsunami, and t_{0-c} for the leading wavefront, for Tsunami Squares and ROMS. κ and τ are depicted as error bars.

Tsunami Squares currently only uses the vertical uplift in its initial wave conditions. Song et al. (2008, 2017) argues for the importance of horizontal seafloor motion during tsunamigenesis, both in additional bulk displacements of water due to bathymetric gradients, and also in kinetic energy transfer to the ocean. The incorporation of this horizontal energy transfer will also be a future improvement of the source model.

5.2. Simulated Inundation

Figure 11 shows a comparison between the inundation observed during the 2011 tsunami ([dataset] National Geophysical Data Center / World Data Service) and the Tsunami Squares simulation. We adopt the language of Jolliffe and Stephenson (2012). Red cells indicate regions where inundation was observed but not recreated in simulation (a forecast "Miss"), green cells indicate agreement between observation and simulation (a forecast "Success"), and blue cells represent areas where inundation was not observed, but which were inundated in simulation (a forecast "False Alarm"). Most simulated inundation occurred in cells where inundation was observed. However, large amounts of coast had observed inundation where the simulated wave did not flow. Considering the locations where this was most prominent, namely in valleys along the coast in the northern simulation region, it is likely that significant inundation forecasting improvements can be made by using a higher-resolution topography dataset. While the NOAA ETOPO1 dataset is sufficient for waves distant to the coast, one arc minute resolution is insufficient for simulating the inundation and runup that occurs in narrow valleys.

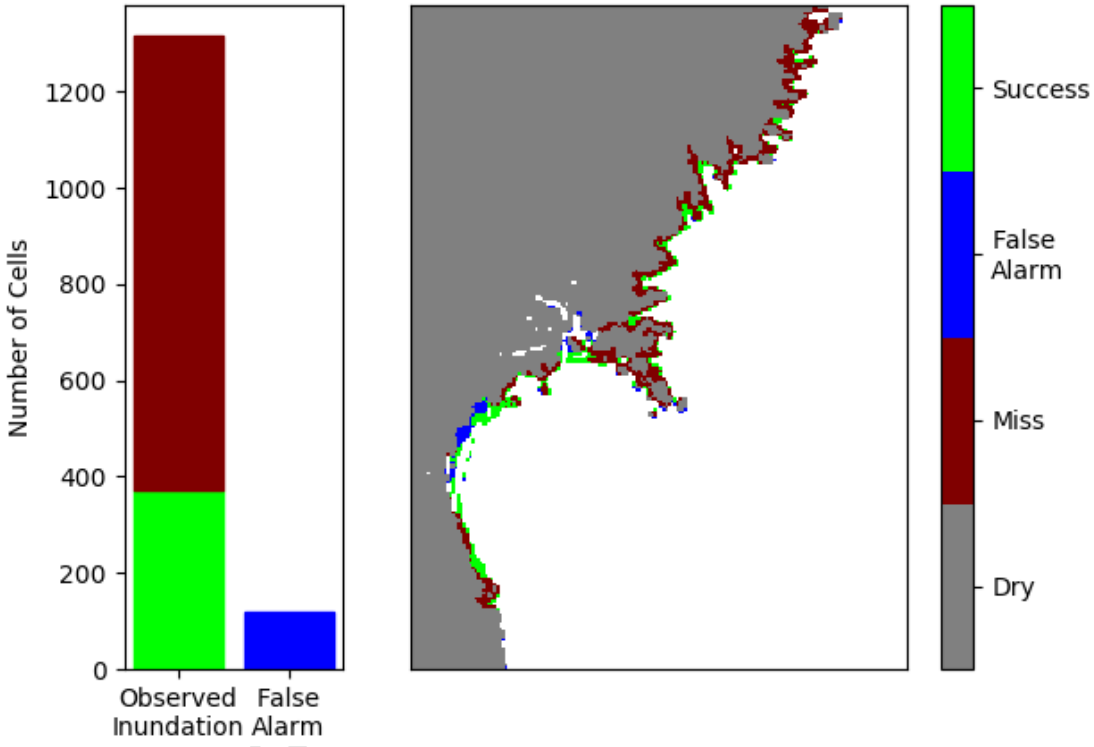

Figure 11: Inundation of the Tohoku coastline from the 2011 tsunami and a Tsunami Squares simulated recreation. Red cells indicate regions where inundation was observed but not recreated in simulation (a forecast "Miss"), green cells indicate agreement between observation and simulation (a forecast "Success"), and blue cells represent areas where inundation was not observed, but which were inundated in simulation (a forecast "False Alarm"). Improvements can be made in using higher-resolution topography data to better simulate run-up in narrow valleys.

6. Conclusion

This article proposes a marriage of the Virtual Quake earthquake simulator and the Tsunami Squares wave simulator for use in statistical tsunami hazard analysis and early warning. Tsunami Squares holds advantages over traditional finite difference methods of simulating the shallow water equations, including needing no special treatment for dry vs. wet cells. Tsunami Squares has been ported from Fortran to C++ in order to leverage GIS and geometry libraries, allowing for simulation on a spherical earth. The new port also allows for multiprocessing, and transitions of simulations between grids of different resolutions.

As a case study, we recreate the 2011 Tohoku earthquake and tsunami. We generate the seafloor uplift of the earthquake, which acts as initial conditions for Tsunami Squares, from the Okada greens functions and fault geometry tools packaged with the Virtual Quake earthquake simulator. We replicate the fault geometry and slip distributions outlined by Satake et al. (2013). The simulated ocean surface then reflects this seafloor displacement.

We validate our simulation against NOWPHAS buoy wave heights during the 2011 Tohoku Tsunami, as well as coastal inundation levels. In comparison to a simulation produced using the open source ROMS simulator, we find similar performance in wave amplitude, with improvement needed in wave arrival times. This will be rectified through the inclusion of time dependence in the tsunami source model.

7. Data Availability

The version of Tsunami Squares used in this research, TsunamiSquares++, can be found at `https://doi.org/10.5281/zenodo.2635777` (Wilson et al., 2019).

The Virtual Quake libraries used for generating the seafloor uplift are hosted by the Computational Infrastructure for Geodynamics at `https://geodynamics.org/cig/software/vq/` (Wilson et al., 2017).

Bathymetry data used in this research is hosted by the National Oceanic and Atmospheric Administration at `http://dx.doi.org/10.7289/V5C8276M` ([dataset] Amante and Eakins, 2009).

Historic tsunami inundation data is from the National Geophysical Data Center / World Data Service Global Historical Tsunami Database. It is hosted at https://data.nodc.noaa.gov/cgi-bin/iso?id=gov.noaa.ngdc.mgg.hazards:G02151 ([dataset] National Geophysical Data Center / World Data Service)

The NOWPHAS buoy data used in this research was observed by the Port and Harbor Bureau of the Ministry of Land, Infrastructure and Transport of Japan, and was processed at the Port and Airport Technology Research Institute. It is hosted at https://nowphas.mlit.go.jp/prg/pastdata/static/sub311.htm ([dataset] Real-time NOWPHAS, 2011)

8. Acknowledgments

This research was supported by NASA grant NNX17AI32G to UC Davis and NASA grant NNX12A22G.

The authors thank the Computational Infrastructure for Geodynamics (http://geodynamics.org) which is funded by the National Science Foundation awards EAR-0949446 and EAR-1550901.

The authors thank Tony Song for providing the ROMS simulation data used as a comparison. ROMS is available from https://www.myroms.org.

References

Able M, Kemper N, R. T. (2012). Review of natural catastrophes in 2011: Earthquakes result in record loss year. Retrieved: April 28, 2016, url: http://www.munichre.com/en/media-relations/publications/press-releases/2012/2012-01-04-press-release/index.html.

Aida, I. (1978). Reliability of a tsunami source model derived from fault parameters. *Journal of Physics of the Earth*, 26(1):57–73.

Ammon, C. J., Ji, C., Thio, H.-K., Robinson, D., Ni, S., Hjorleifsdottir, V., Kanamori, H., Lay, T., Das, S., Helmberger, D., et al. (2005). Rupture process of the 2004 Sumatra-Andaman earthquake. *Science*, 308(5725):1133–1139.

[dataset] Amante, C. and Eakins, B. (2009). ETOPO1 1 arc-minute global relief model: Procedures, data sources and analysis. NOAA technical memorandum NESDIS NGDC-24. National Geophysical Data Center, NOAA. doi: 10.7289/V5C8276M, url: http://dx.doi.org/10.7289/V5C8276M, Accessed: April 29, 2019.

[dataset] National Geophysical Data Center / World Data Service. NCEI/WDS, Global Historical Tsunami Database. NOAA National Centers for Environmental Information. doi: 10.7289/V5PN93H7, url: https://data.nodc.noaa.gov/cgi-bin/iso?id=gov.noaa.ngdc.mgg.hazards:G02151, Accessed: April 12, 2019.

[dataset] Real-time NOWPHAS (2011). Tsunami observation data from the Tohoku region Pacific ocean earthquake. Port Authority of the Ministry of Land, Infrastructure and Transport of Japan. url: https://nowphas.mlit.go.jp/prg/pastdata/static/sub311.htm, Accessed: April 29, 2019.

Fujii, Y. and Satake, K. (2013). Slip distribution and seismic moment of the 2010 and 1960 chilean earthquakes inferred from tsunami waveforms and coastal geodetic data. *Pure and Applied Geophysics*, 170(9-10):1493–1509.

Hayes, G., Myers, E., Dewey, J., Briggs, R., Earle, P., Benz, H., Smoczyk, G., Flamme, H., Barnhart, W., Gold, R., , and Furlong, K. (2017). Tectonic summaries of magnitude 7 and greater earthquakes from 2000 to 2015: U.s. geological survey open-file report 20161192. Technical report. US Geological Survey. doi: 10.3133/ofr20161192, url: https://pubs.er.usgs.gov/publication/ofr20161192.

Imamura, F. (1996). Review of tsunami simulation with a finite difference method. *Long-wave runup models*, pages 25–42.

Jolliffe, I. T. and Stephenson, D. B. (2012). *Forecast Verification: A Practitioner's Guide in Atmospheric Science*. John Wiley & Sons.

Lay, T., Kanamori, H., Ammon, C. J., Nettles, M., Ward, S. N., Aster, R. C., Beck, S. L., Bilek, S. L., Brudzinski, M. R., Butler, R., et al. (2005). The great Sumatra-Andaman earthquake of 26 December 2004. *Science*, 308(5725):1127–1133.

Mori, N., Takahashi, T., and Group, . T. E. T. J. S. (2012). Nationwide post event survey and analysis of the 2011 Tohoku earthquake tsunami. *Coastal Engineering Journal*, 54(01):1250001.

Nelson, A. R., Kelsey, H. M., and Witter, R. C. (2006). Great earthquakes of variable magnitude at the Cascadia subduction zone. *Quaternary Research*, 65(3):354–365.

Okada, Y. (1992). Internal deformation due to shear and tensile faults in a half-space. *Bulletin of the Seismological Society of America*, 82(2):1018–1040.

Rundle, J. B. and Jackson, D. D. (1977). Numerical simulation of earthquake sequences. *Bulletin of the Seismological Society of America*, 67(5):1363–1377.

Rundle, J. B., Rundle, P. B., Donnellan, A., Li, P., Klein, W., Morein, G., Turcotte, D., and Grant, L. (2006). Stress transfer in earthquakes, hazard estimation and ensemble forecasting: Inferences from numerical simulations. *Tectonophysics*, 413(1-2):109–125.

Sachs, M. K., Heien, E. M., Turcotte, D. L., Yikilmaz, M. B., Rundle, J. B., and Kellogg, L. H. (2012). Virtual California earthquake simulator. *Seismological Research Letters*, 83(6):973–978.

Satake, K., Fujii, Y., Harada, T., and Namegaya, Y. (2013). Time and space distribution of coseismic slip of the 2011 Tohoku earthquake as inferred from tsunami waveform data. *Bulletin of the Seismological Society of America*, 103(2B):1473–1492.

Satake, K., Shimazaki, K., Tsuji, Y., and Ueda, K. (1996). Time and size of a giant earthquake in Cascadia inferred from Japanese tsunami records of January 1700. *Nature*, 379(6562):246.

Schultz, K. W., Yoder, M. R., Wilson, J. M., Heien, E. M., Sachs, M. K., Rundle, J. B., and Turcotte, D. L. (2018). Parametrizing physics-based earthquake simu-

lations. In *Earthquakes and Multi-hazards Around the Pacific Rim, Vol. I*, pages 75–84. Springer.

Shennan, I., Bruhn, R., and Plafker, G. (2009). Multi-segment earthquakes and tsunami potential of the aleutian megathrust. *Quaternary Science Reviews*, 28(1):7 – 13.

Song, Y. T., Fu, L.-L., Zlotnicki, V., Ji, C., Hjorleifsdottir, V., Shum, C., and Yi, Y. (2008). The role of horizontal impulses of the faulting continental slope in generating the 26 December 2004 tsunami. *Ocean Modelling*, 20(4):362–379.

Song, Y. T., Mohtat, A., and Yim, S. C. (2017). New insights on tsunami genesis and energy source. *Journal of Geophysical Research: Oceans*, 122(5):4238–4256.

Wang, J., Ward, S. N., and Xiao, L. (2015a). Numerical modelling of rapid, flow-like landslides across 3-d terrains: a Tsunami Squares approach to El Picacho landslide, El Salvador, September 19, 1982. *Geophysical Journal International*, 201(3):1534–1544.

Wang, J., Ward, S. N., and Xiao, L. (2015b). Numerical simulation of the December 4, 2007 landslide-generated tsunami in Chehalis Lake, Canada. *Geophysical Journal International*, 201(1):372–376.

Ward, S. N. (2011). Tsunami. In *Encyclopedia of Solid Earth Geophysics*, pages 1473–1493. Springer Science & Business Media.

Wilson, J. M., Schultz, K., Heien, E., Sachs, M., and Rundle, J. (2017). Virtual Quake v3.1.1. doi: `http://doi.org/10.5281/zenodo.1098321`.

Wilson, J. M., Schultz, K. W., and Ward, S. N. (2019). TsunamiSquares++ v1.0.0. doi: `http://doi.org/10.5281/zenodo.2635777`.

Xiao, L., Ward, S. N., and Wang, J. (2015). Tsunami Squares approach to landslide-generated waves: Application to Gongjiafang landslide, Three Gorges Reservoir, China. *Pure and Applied Geophysics*, 172(12):3639–3654.

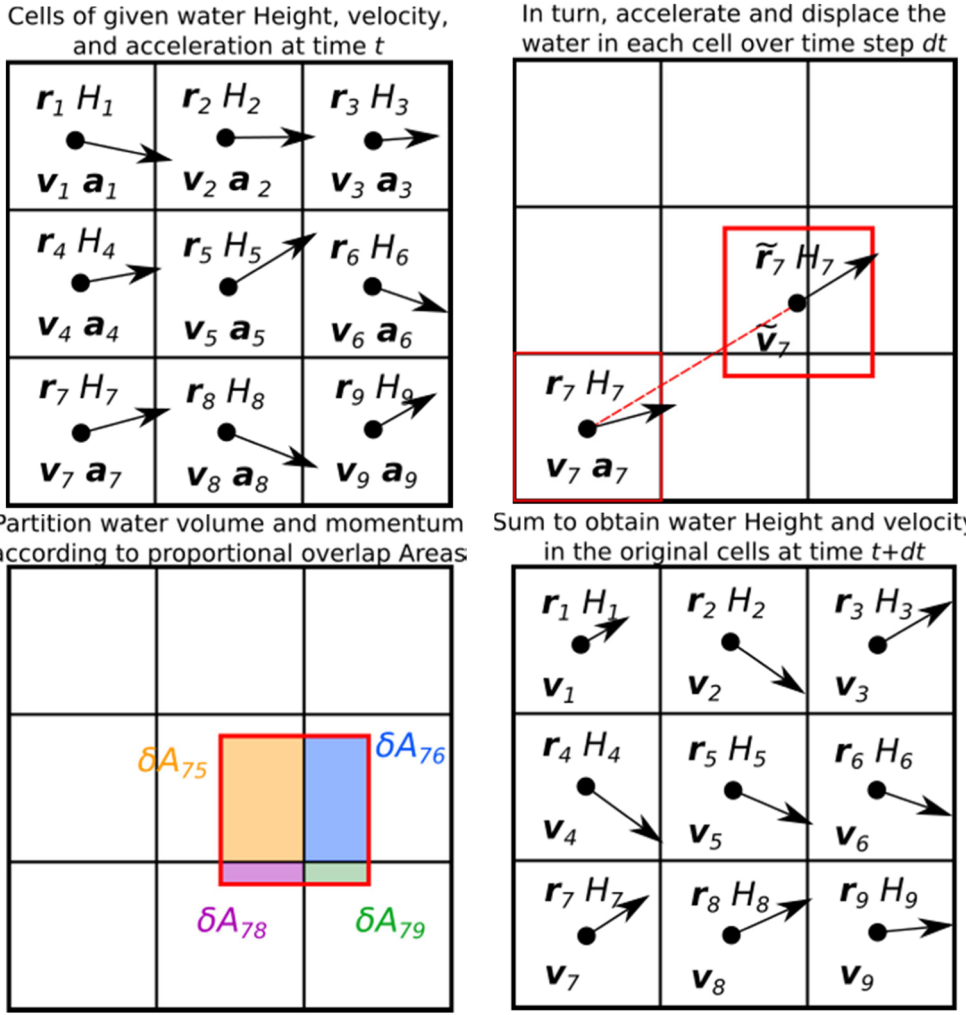
Cells of given water Height, velocity, and acceleration at time t
r1 H1
v1 a1
r2 H2
v2 a 2
r3 H3
v3 a3
r4 H4
v4 a4
r5 H5
v5 a5
r6 H6
v6 a6
r7 H7
v7 a7
r8 H8
v8 a8
r9 H9
v9 a9
In turn, accelerate and displace the water in each cell over time step dt
r̃7 H7
ṽ7
r7 H7
v7 a7
Partition water volume and momentum according to proportional overlap Areas
δA75
δA76
δA78
δA79
Sum to obtain water Height and velocity in the original cells at time t+dt
r1 H1
v1
r2 H2
v2
r3 H3
v3
r4 H4
v4
r5 H5
v5
r6 H6
v6
r7 H7
v7
r8 H8
v8
r9 H9
v9

Figure 1

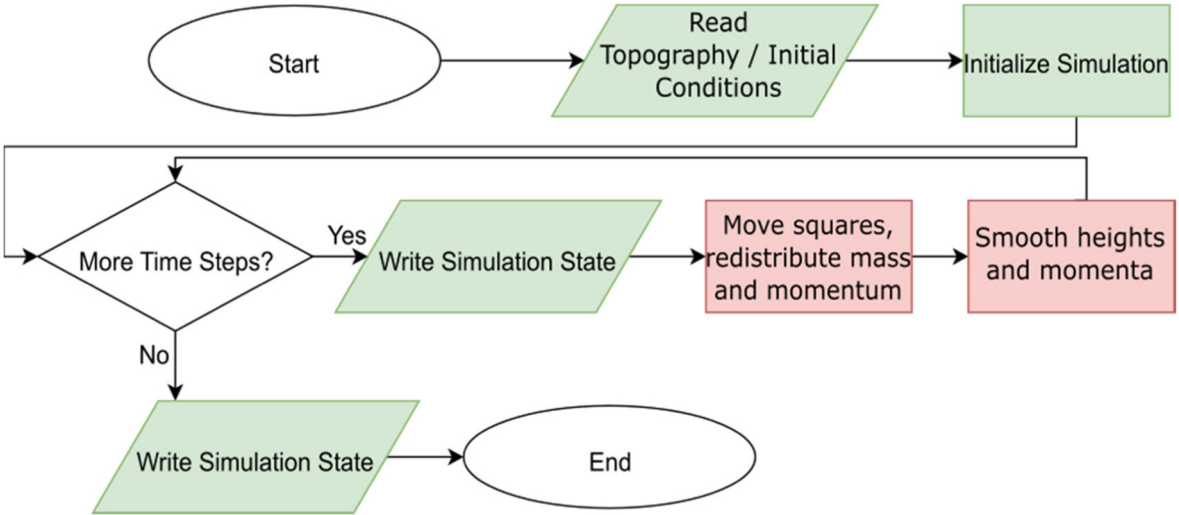
Start
Read
Topography / Initial
Conditions
Initialize Simulation
More Time Steps?
Yes
Write Simulation State
Move squares,
redistribute mass
and momentum
Smooth heights
and momenta
No
Write Simulation State
End

Figure 2

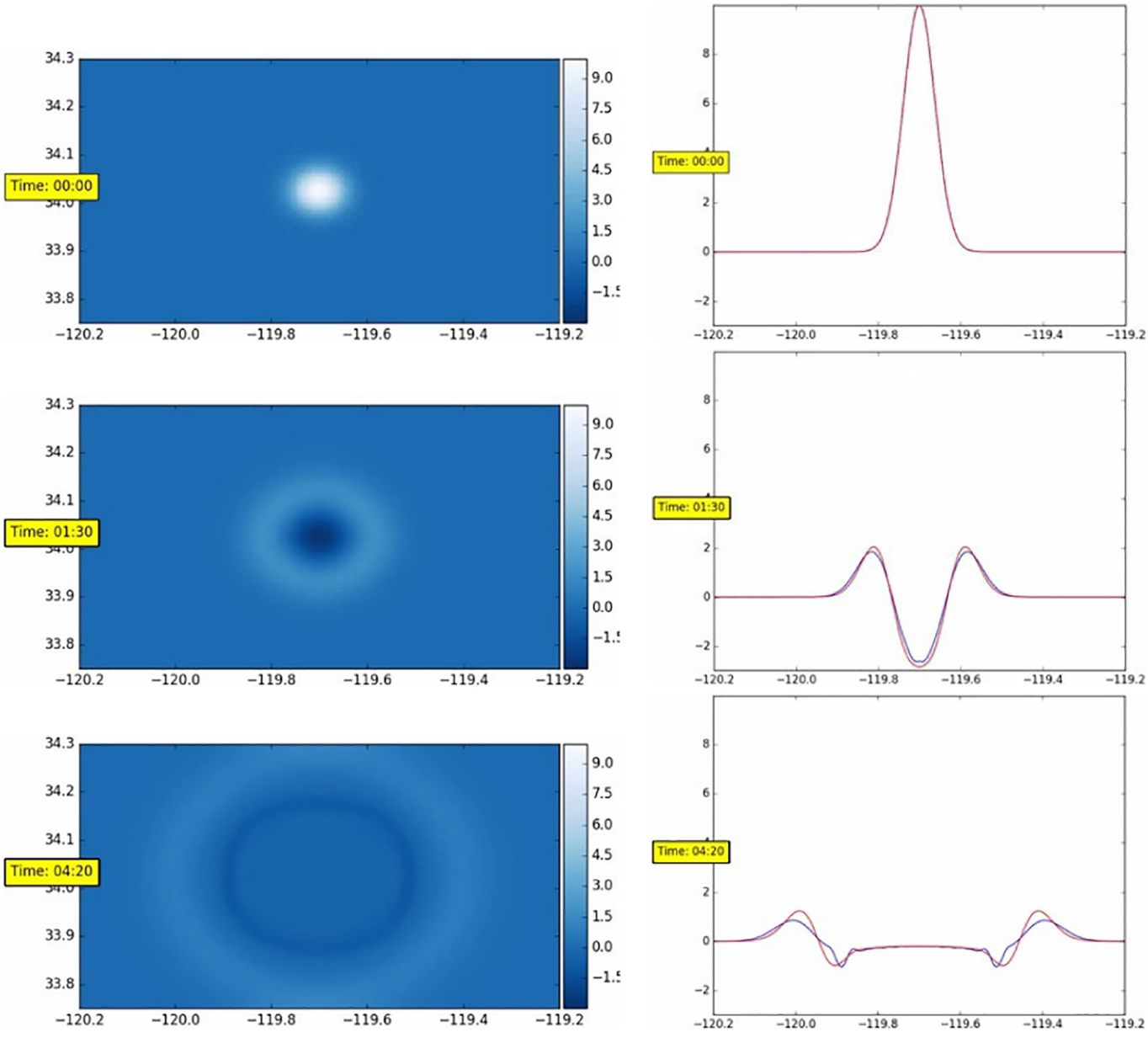
Time: 00:00
Time: 01:30
Time: 04:20
34.3
34.2
34.1
33.9
33.8
−120.2
−120.0
−119.8
−119.6
−119.4
−119.2
9.0
7.5
6.0
4.5
3.0
1.5
0.0
8
6
2
0
−2

Figure 3

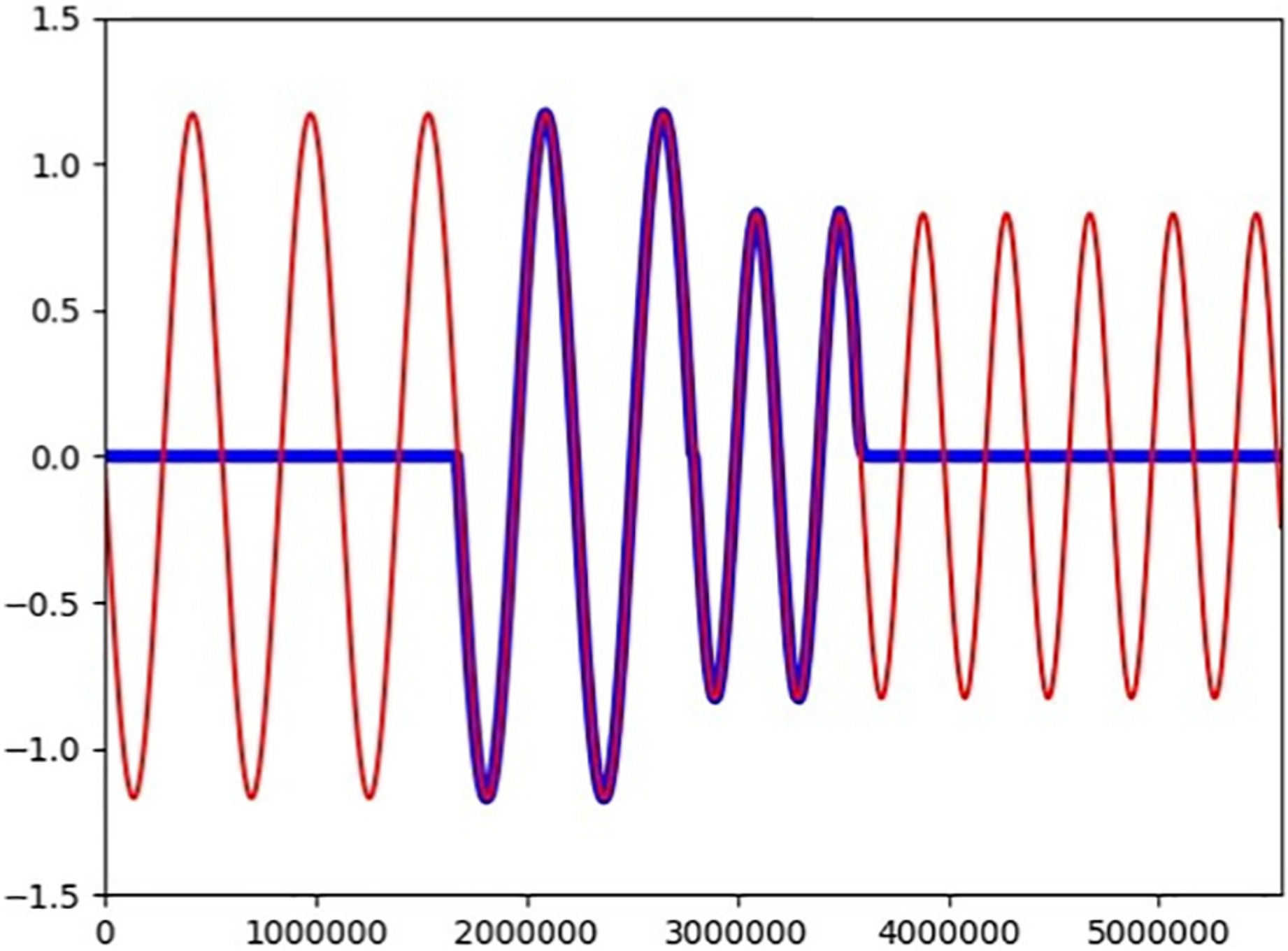
1.5
1.0
0.5
0.0
−0.5
−1.0
−1.5
0
1000000
2000000
3000000
4000000
5000000

Figure 4

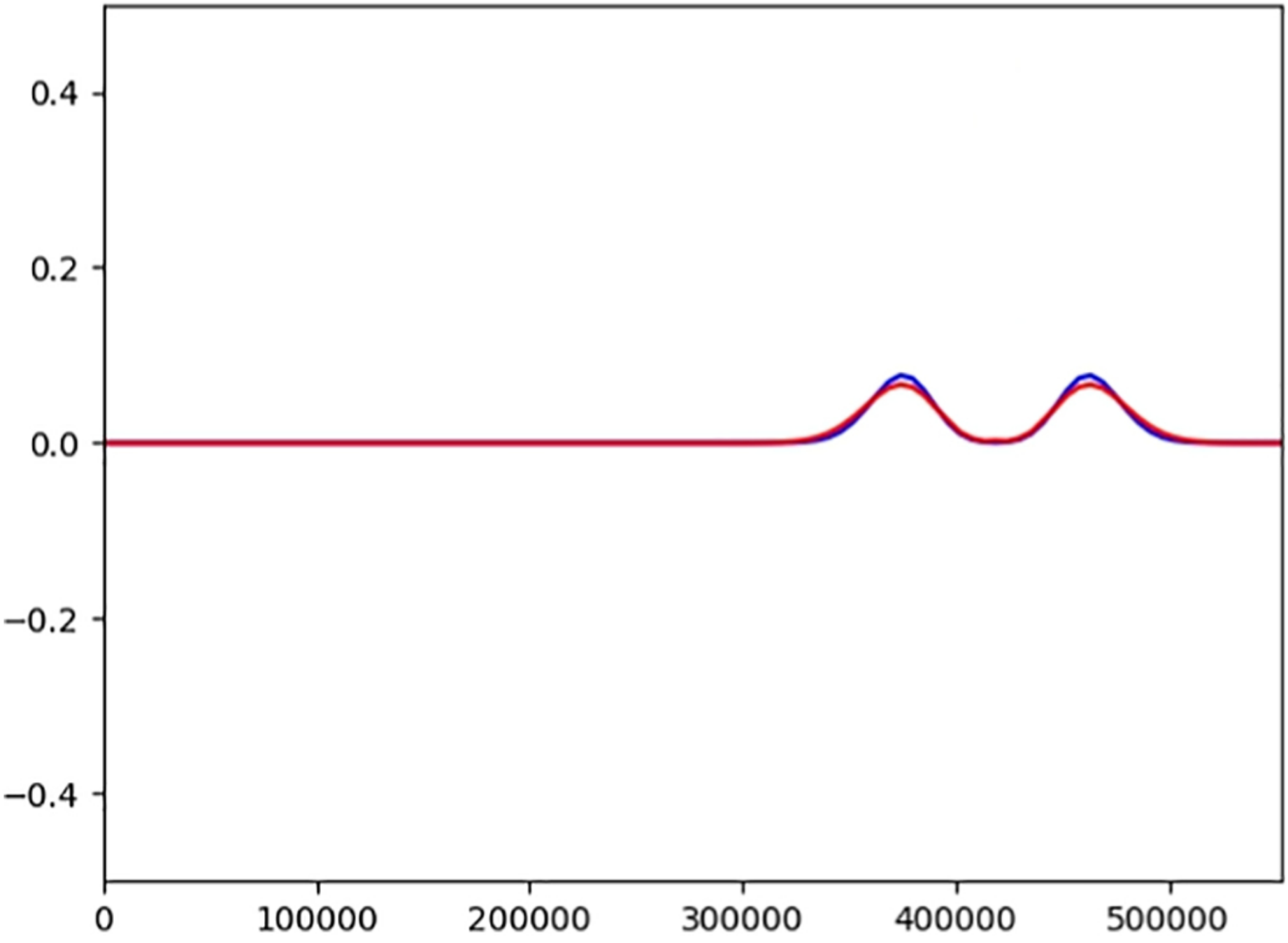

Figure 5

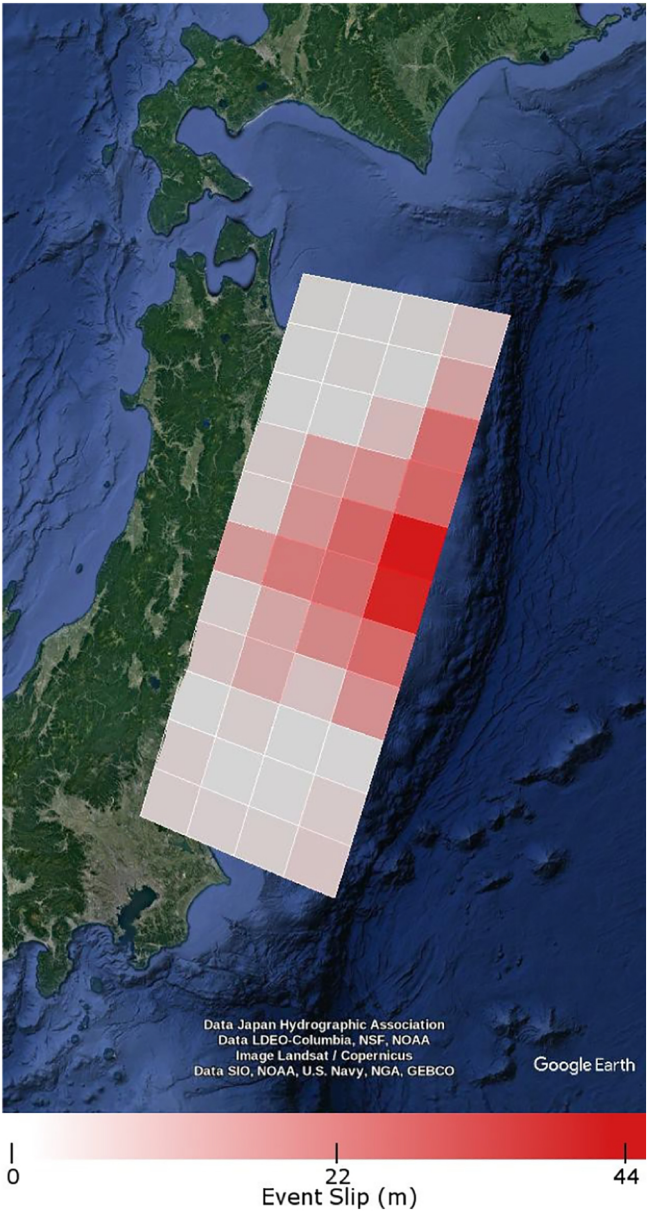
Data Japan Hydrographic Association
Data LDEO-Columbia, NSF, NOAA
Image Landsat / Copernicus
Data SIO, NOAA, U.S. Navy, NGA, GEBCO
Google Earth
0
22
44
Event Slip (m)

Figure 6

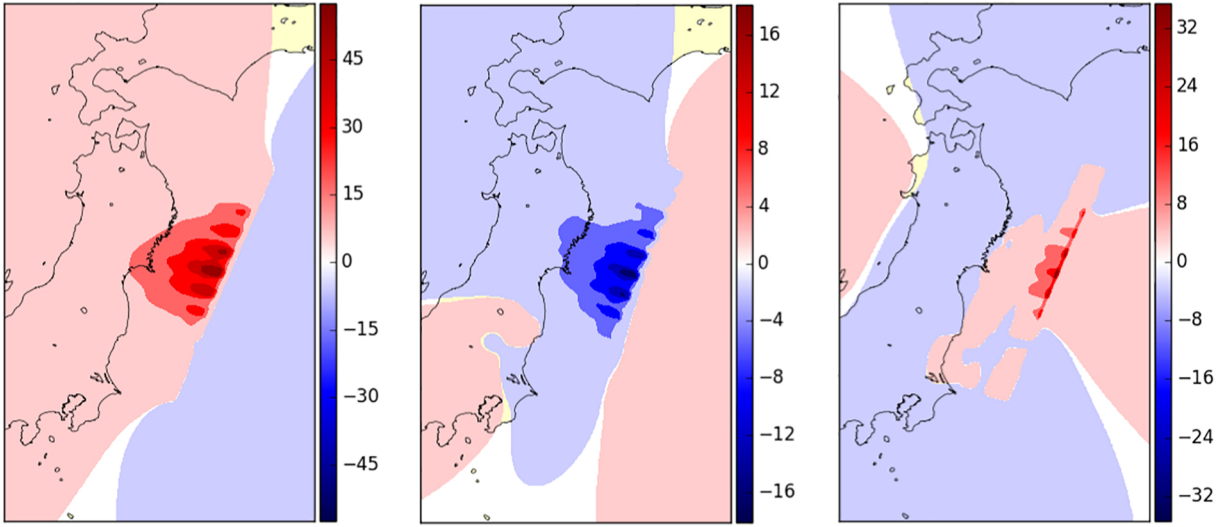
East Displacement (m)
45
30
15
0
−15
−30
−45
North Displacement (m)
16
12
8
4
0
−4
−8
−12
−16
Vertical Displacement (m)
32
24
16
8
0
−8
−16
−24
−32

Figure 7

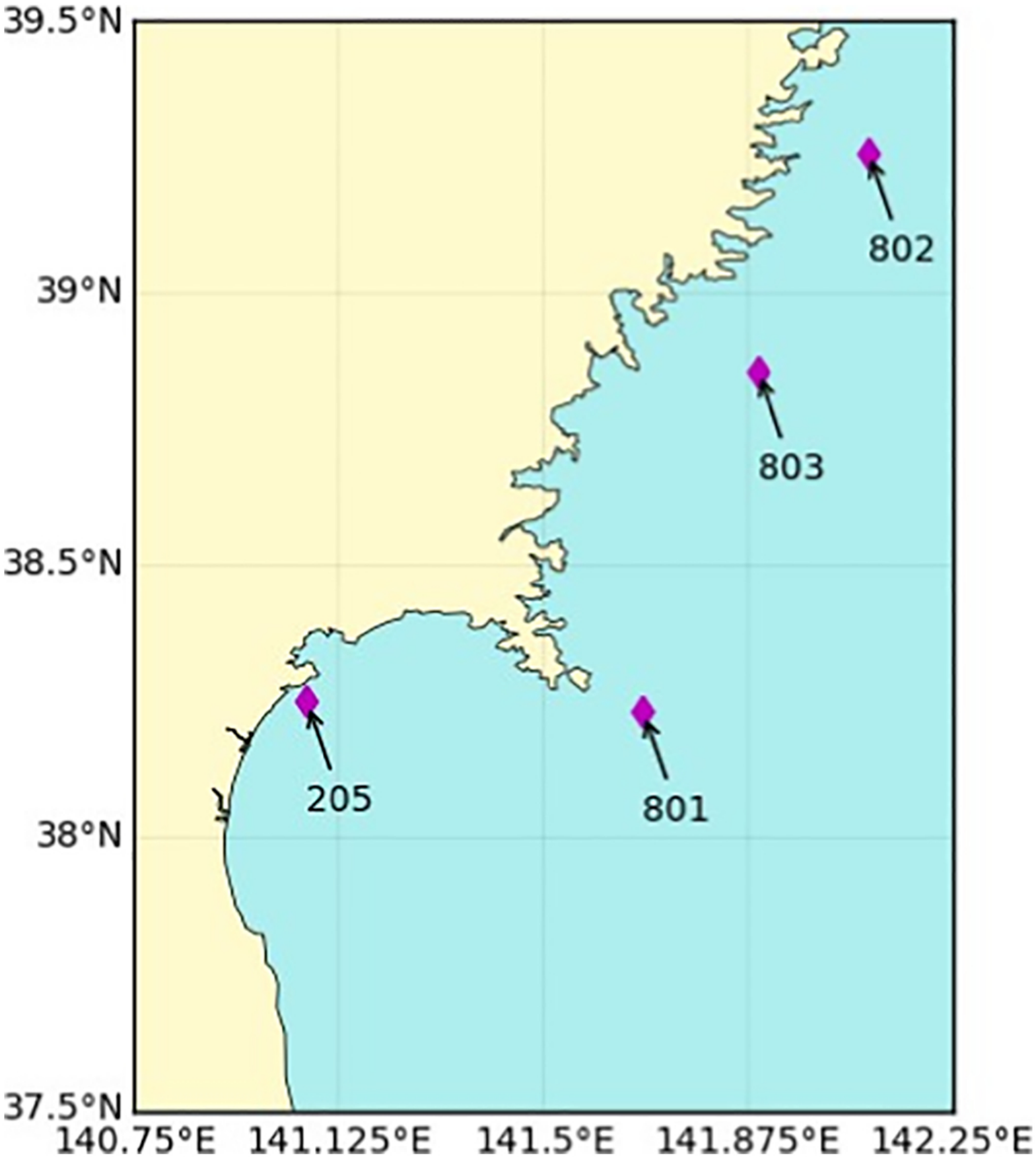
39.5°N
39°N
38.5°N
38°N
37.5°N
140.75°E
141.125°E
141.5°E
141.875°E
142.25°E
802
803
205
801

Figure 8

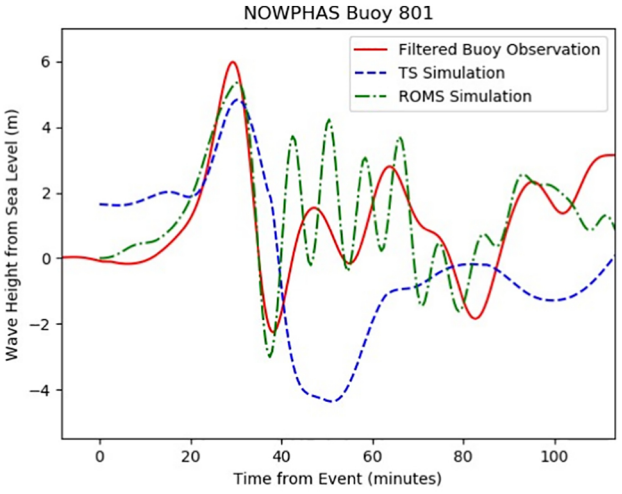
NOWPHAS Buoy 801
Filtered Buoy Observation
TS Simulation
ROMS Simulation
Wave Height from Sea Level (m)
Time from Event (minutes)

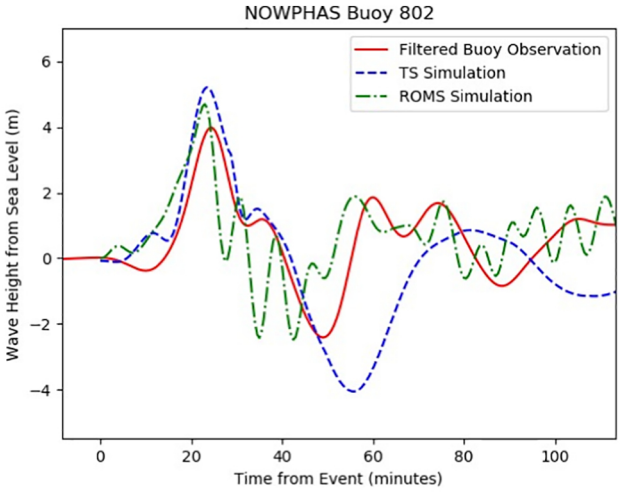
NOWPHAS Buoy 802
Filtered Buoy Observation
TS Simulation
ROMS Simulation
Wave Height from Sea Level (m)
Time from Event (minutes)

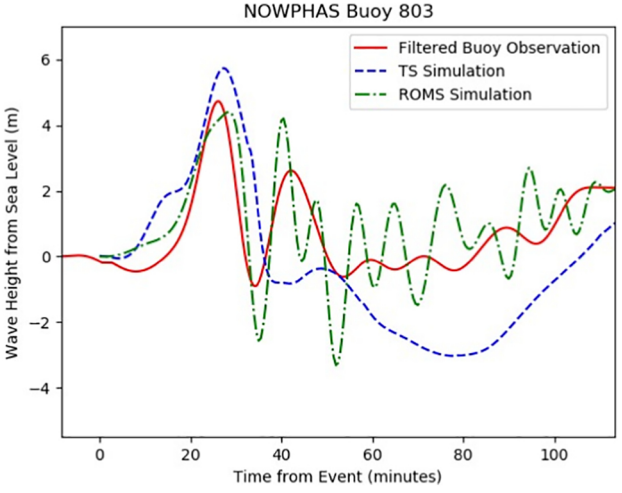
NOWPHAS Buoy 803
Filtered Buoy Observation
TS Simulation
ROMS Simulation
Wave Height from Sea Level (m)
Time from Event (minutes)

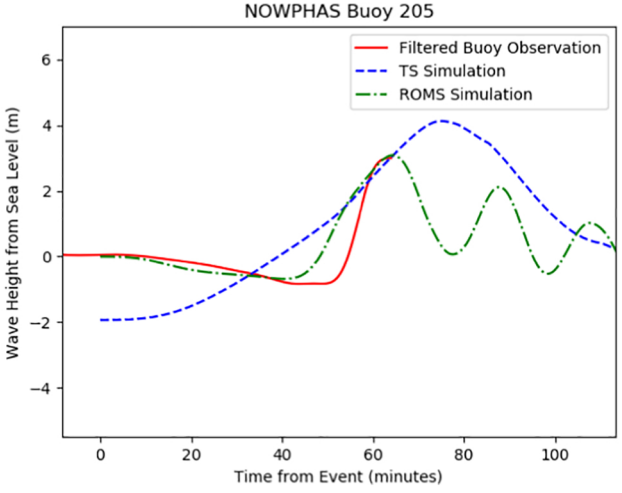
NOWPHAS Buoy 205
Filtered Buoy Observation
TS Simulation
ROMS Simulation
Wave Height from Sea Level (m)
Time from Event (minutes)

Figure 9

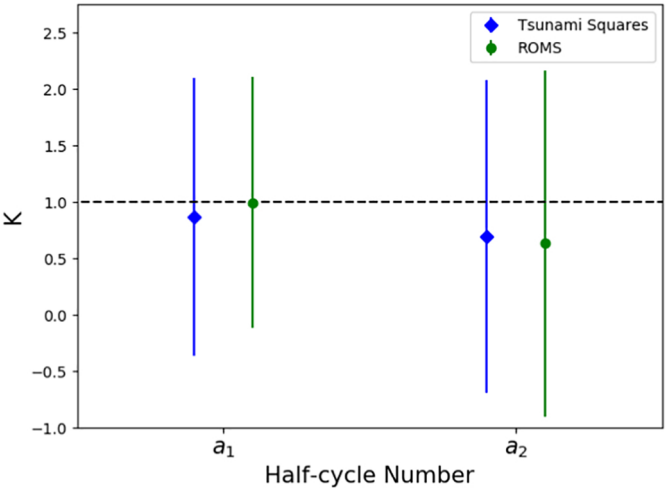
Tsunami Squares
ROMS
2.5
2.0
1.5
1.0
0.5
0.0
−0.5
−1.0
K
a_1
a_2
Half-cycle Number

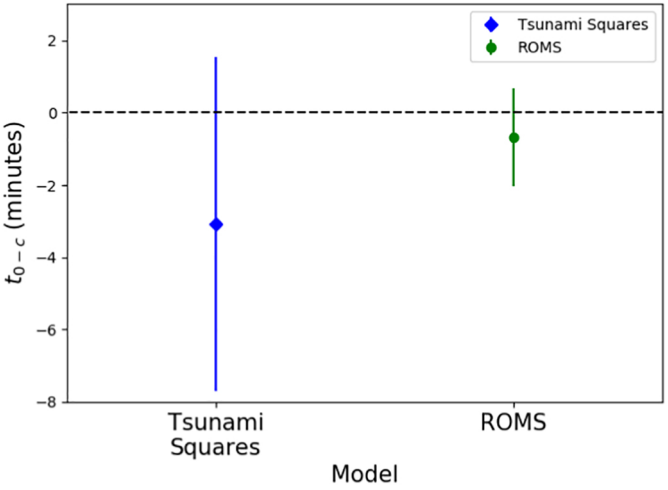
Tsunami Squares
ROMS
2
0
−2
−4
−6
−8
t_{0-c} (minutes)
Tsunami Squares
ROMS
Model

Figure 10

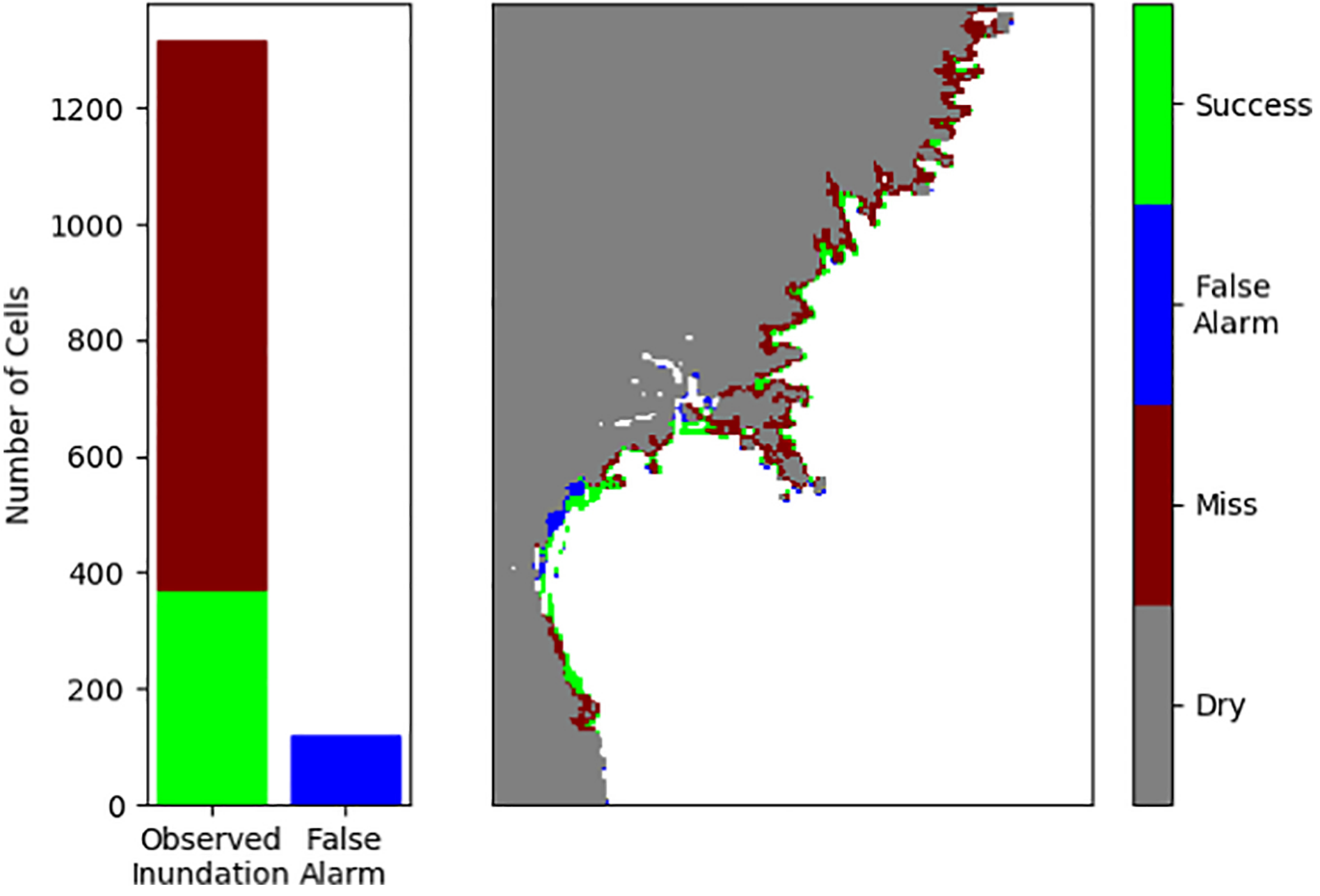
Number of Cells
0
200
400
600
800
1000
1200
Observed Inundation
False Alarm
Success
False Alarm
Miss
Dry

Figure 11